Competition of mixing and segregation in rotating cylinders

Christian M. Dury and Gerald H. Ristow
Fachbereich Physik, Philipps-Universität, Renthof 6, 35032 Marburg, Germany

(Received 5 March 1998; accepted 1 March 1999)

Using discrete element methods, we study numerically the dynamics of the size segregation process of binary particle mixtures in three-dimensional rotating drums, operated in the continuous flow regime. Particle rotations are included and we focus on different volume filling fractions of the drum to study the interplay between the competing phenomena of mixing and segregation. It is found that segregation is best for a more than half-filled drum due to the nonzero width of the fluidized layer. For different particle size ratios, it is found that radial segregation occurs for any arbitrary small particle size difference and the final amount of segregation shows a linear dependence on the size ratio of the two particle species. To quantify the interplay between segregation and mixing, we investigate the dynamics of the center of mass positions for each particle component. Starting with initially separated particle groups we find that no mixing of the component is necessary in order to obtain a radially segregated core. © *1999 American Institute of Physics.*
[S1070-6631(99)03106-2]

I. INTRODUCTION

When granular materials are placed in rotating cylinders, different flow dynamics are observed. The major portion of the particles undergoes a solid body rotation by following the cylinder motion. Close to the free surface, a downhill particle flow is observed where the flow dynamics depends on the rotation speed of the cylinder.[1–3] For low rotation speeds, the surface flow consists of individual avalanches called the discrete avalanche regime. With increasing rotation speed the separation time of avalanches will decrease until no individual avalanches are detectable. A nearly constant particle flow is found along the free surface and this regime is consequently termed the continuous flow regime. Close to this transition, the surface can be well approximated by a straight plane, which can be used to determine the surface angle. For even higher rotation speeds, cascading, cataracting and centrifuging particle motion is also observed.[1] Experiments performed in the discrete avalanche regime using mono-disperse particles show that the mixing time depends strongly on the volume filling fraction of the cylinder and no mixing is seen for an exactly half-filled cylinder.[4] A theoretical description could be given which is based on the mixing between wedges.[4–6] On the other hand, when a mixture of particles which differ in size or density are placed in a rotating cylinder, the denser or smaller particles will concentrate in a central region close to the free surface after only a few rotations, which is termed *radial segregation*. This was studied experimentally and numerically for varying size ratios[7–11] and density ratios.[12–14] The amount and direction of segregation depends on the rotation rate.[1] However, radial segregation is always observed in the continuous flow regime, regardless of the filling fraction of the cylinder and we are investigating numerically the interplay of the two competing phenomena of mixing and segregation, a problem first studied by Rose[15] and restated by Behringer.[16] We are particularly interested in the dependence of the total amount of segregation on the size ratio of glass beads and how the segregation behaves for size ratios close to one.

The paper is organized in the following way: After a brief motivation of the physical system in mind in the beginning of the next section, we will explain our numerical model and the physical meaning of the parameters in the remainder of Sec. II. In order to model the dynamics of glass beads correctly with our model, we have to include rolling friction. The details of our implementation are given in the appendix. We define an order parameter which allows to quantify the amount and the speed of radial segregation. The dynamics of this order parameter are discussed in detail in Sec. III for different particle size ratios and as a function of the volume filling fraction of the cylinder. In addition, we start with an initial configuration similar to the one used in the original experiment on the mixing of mono-disperse particles[4] to demonstrate how the radial segregation competes with the mixing process.

II. MOTIVATION AND NUMERICAL MODEL

In many radial and axial segregation experiments, one of the components are glass beads. They are commercially available in large quantities and can easily be sieved to nearly uniform size distribution. When sufficiently large, the cohesion forces are negligible. In the continuous flow regime, the dynamic angle of repose for glass spheres seems to be independent of the bead diameter for a range of rotation speeds of the cylinder as long as the free surface remains flat.[17,18] Since they are nearly perfectly round, particle rotations are an important degree of freedom and cannot be neglected in a theoretical or numerical description.

We investigate the radial segregation process numerically by using a cylinder with periodic boundary conditions along the rotational axis. Using a numerical method gives us the freedom to vary particle size ratios freely, whereas in experiments only a limited number of particle diameters and densities is available. In order to determine the minimal

length of this cylinder, i.e., to avoid artifacts due to the periodic boundary conditions, we have investigated the range of the boundary effects in a previous study.[18]

A. Forces during collisions

Each particle i is approximated by a sphere with radius R_i. Only contact forces during collisions are considered and the particles are allowed to rotate; we also include rolling resistance to our model to correctly describe the dynamics of glass beads (see the appendix). The forces acting on particle i during a collision with particle j are

$$F_{ij}^n = -\tilde{Y}(R_i + R_j - \mathbf{r}_{ij}\hat{n}) - \gamma_n \mathbf{v}_{ij}\hat{n}, \tag{1}$$

in the normal direction $(\hat{n})$ and

$$F_{ij}^s = -\min(\gamma_s \mathbf{v}_{ij}\cdot\hat{s}(t), \mu|F_{ij}^n|), \tag{2}$$

in the tangential direction $(\hat{s})$ of shearing. In Eq. (1), γ_n represents the dynamic damping coefficient and Eq. (2) γ_s represents the dynamic friction force in the tangential direction. $\mathbf{r}_{ij}$ represents the vector joining both centers of mass, $\mathbf{v}_{ij}$ represents the relative motion of the two particles and $\tilde{Y}$ is related to the Young Modulus of the investigated material. Dynamic friction in this model is defined to be proportional to the relative velocity of the particles in the tangential direction.

During particle–wall contacts, the wall is treated as a particle with infinite mass and radius. In the normal direction, Eq. (1) is applied, whereas in the tangential direction, the static friction force,

$$\tilde{F}_{ij}^s = -\min\left(k_s \int \mathbf{v}_{ij}\cdot\hat{s}(t)dt, \mu|F_{ij}^n|\right), \tag{3}$$

is used. This is motivated by the observation that when particles flow along the free surface, they dissipate most of their energy in collisions and can come to rest in voids left by other particles. This is not possible at the cylinder walls. In order to avoid additional artificial particles at the walls we use a static friction law to avoid slipping and allowing for a static surface angle when the rotation is stopped. Both tangential forces are limited by the Coulomb criterion, see Eqs. (2) and (3), which states that the magnitude of the tangential force cannot exceed the magnitude of the normal force multiplied by the friction coefficient μ. Even though the experimentally measured friction coefficient for fresh glass beads is $\mu = 0.092$[19] this can only be viewed as a lower bound in our case due to the wear of material caused by the uncountable bead collisions in the course of the experiment. For particle–particle collisions we use $\mu = 0.19$, and for particle–wall collisions, $\mu_w = 0.6$. The coefficient of restitution for wall collisions is set to 0.97 and to 0.831 for particle–particle collisions, which are the measured values for glass beads[19] and the density was set to $\rho = 2.5\,\mathrm{g/cm^3}$. In order to save computer time, we set $\tilde{Y}$ to 6×10^4 Pa m which is about one order of magnitude softer than glass, but we checked that this has no effect on the investigated properties of the material, e.g., by measuring the dynamic angle of repose as a function of rotation speed. This gives a contact time during collisions of 1.1×10^{-6} s, which is still quite small. The total number of particles we used were up to 17000.

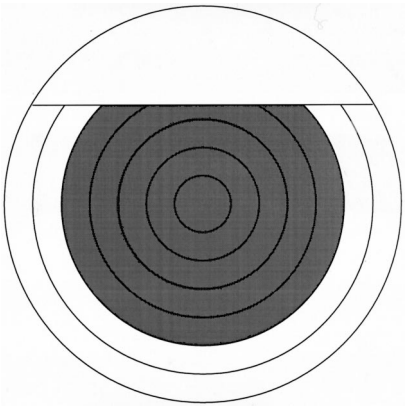

FIG. 1. Cross section through a more than half-filled cylinder.

B. Order parameter

To compare the quality and speed of the segregation of different runs with different parameters, a suitable order parameter is needed. For this we divide the cylinder with diameter D into n concentric hollow cylinders with thickness $\Delta = D/2n$ and measure the number density of the smaller particles, ρ_i, in each hollow cylinder $i = 1, \ldots, n$ (see Fig. 1). We choose as such an order parameter q the sum over all positive deviations of ρ_i above the mean number density,

$$\rho_0 = \frac{\text{Number of small particles}}{\pi(D/2)^2 f},$$

in a cylinder with a filling fraction f, normalized with respect to the ideally segregated case, where all inner cylinders $i = 1, \ldots, c$ are composed only out of small particles shown in gray in Fig. 1 and in the outer cylinders $i = c+1, \ldots, n$ only out of large particles; see also Ref. 11. To get reasonable results, we take Δ to be of the order of the diameter of the larger particles, which gives in our case $n = 11$. For smaller values of n, the spatial resolution gets worse and for higher n fluctuations become more pronounced, since there would be ''empty'' shells with no particle centers in it. For varying n around 11, q has an over-all error of 0.03 for $n \in [9,20]$.

III. SIZE SEGREGATION

For our simulation we use a cylinder with a diameter of $D = 7$ cm and a length of 2.5 cm. It is filled with a binary mixture of large beads having a radius of $R = 1.5$ mm and small beads $r \in \{0.75\text{ mm}, 1.0\text{ mm}, 1.25\text{ mm}\}$. The small particles can have a concentration of 50% or 33% by volume. The aspect ratio of the drum diameter D to the average particle diameter $2r$ is $D/(2r) = 28$ which is of the order of laboratory experiments, where we have $D/(2r) = 25$ up to 40 for the example in Ref. 1. For the rotation rate of the drum used throughout this paper, $\Omega = 15$ rpm, we are in the continuous flow regime with a flat free surface, and the Froude number is

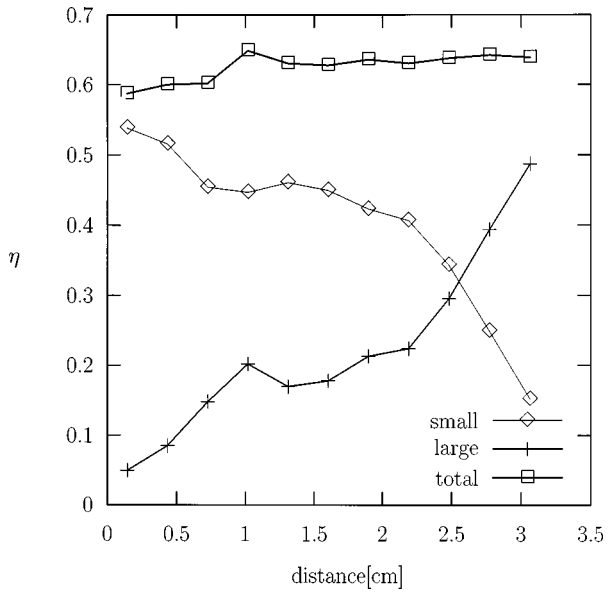

FIG. 2. Volume fraction of small and large particles in each cylinder for a volume filling fraction of 66.4%.

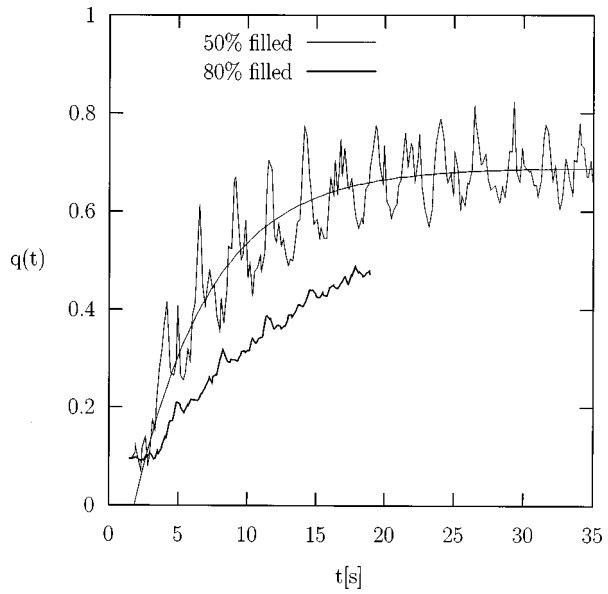

FIG. 3. Typical time series of the order parameter q for two different filling fractions of the cylinder with 1.0 mm and 1.5 mm beads.

$$Fr=\frac{\Omega^2 L}{g}=8.8\times 10^{-3},$$

so we can neglect inertia effects.

A. Packing fraction

The volume filling fraction is defined as the ratio of the volume occupied by the granular material to the cylinder volume, reading as

$$f=\frac{V_{\text{occupied}}}{(D/2)^2\pi L}, \tag{4}$$

where the occupied volume depends on the packing fraction η via

$$V_{\text{occupied}}=\frac{1}{\eta}\sum_{\text{all particles}}\frac{4}{3}r^3\pi. \tag{5}$$

Hence, the packing fraction η is determined by

$$\eta=\frac{\Sigma_{\text{all particles}}(4/3)\,r^3\pi}{f\cdot(D/2)^2\pi L}; \tag{6}$$

i.e., filling the drum with a certain filling fraction and summing up the volumes of each particle. We found that this packing fraction η does not change with the amount of achieved segregation. However, η depends on the particle size ratio of small and large particles $\Phi:=r/R$ giving $\eta=0.65$ for $\Phi=0.5$ with a monotonic decrease to $\eta=0.593$ for $\Phi=0.96$. In Fig. 2 we used $\Phi=0.75\,\text{mm}/1.5\,\text{mm}=0.5$ and the cylinder was rotated for $2\frac{1}{2}$ revolutions, which gives a nearly complete radial segregation. The small particles, denoted by $\diamond$, are mostly found in the middle of the cylinder, whereas the large particles, denoted by $+$, show a higher concentration in the outer cylinders. Also shown is the total volume occupied by all spheres, denoted by $\square$, which gives an average value in each cylinders of $\eta=0.64$ which is close to the value for a random particle packing.

B. Time evolution of the order parameter

Usually the initial state is a random mixture of small and large particles which gives a value of $q\approx 0$. The order parameter will show a global trend of increasing in time and saturates on the long run when the cylinder rotation is started. A typical time evolution of q using a 50% volume fraction of 1.0 mm smaller particles is shown in Fig. 3. The general trend can be well approximated by an exponential saturating function of the form

$$q(t)=q_\infty(1-e^{-t/t_c}), \tag{7}$$

with a characteristic segregation time t_c and a final amount of segregation q_∞. The best fit to the data points was obtained for the parameters $t_c=(6.1\pm 0.3)$ s and $q_\infty=0.644\pm 0.040$, respectively, which was added to Fig. 3 as a solid line.

When working in the discrete avalanche regime, it was found in experiments[4] and mathematical models[5,6] that the least amount of geometrical mixing is given for a half-filled drum which could be explained by the avalanche mixing of wedges. Peratt and Yorke[5] applied their model also to the continuous avalanche regime by taking the limit of an infinitely thin flowing layer and no change in the angle of repose during the flow. Motivated by these findings, we expected for our setup to get the least geometrical mixing for filling fractions around 50% as well and the strong fluctuations which are most pronounced for a filling fraction of 50% are a clear sign for slow geometrical mixing. The average velocity and the shape of the fluidized layer was, e.g., calculated by Khakhar *et al.*[20]

Fourier-transforming these fluctuations gives main peaks for the 50% and the 80% filled drum at $T=(2.56\pm 0.09)$ s and $T=(3.18\pm 0.15)$ s, albeit the peak for the 80% filled case is much less pronounced than in the 50% case, as is shown in Fig. 4; higher harmonics are also visible. These times were obtained as the peaks in the Fourier-transform and correspond exactly to the time it takes for a particle to

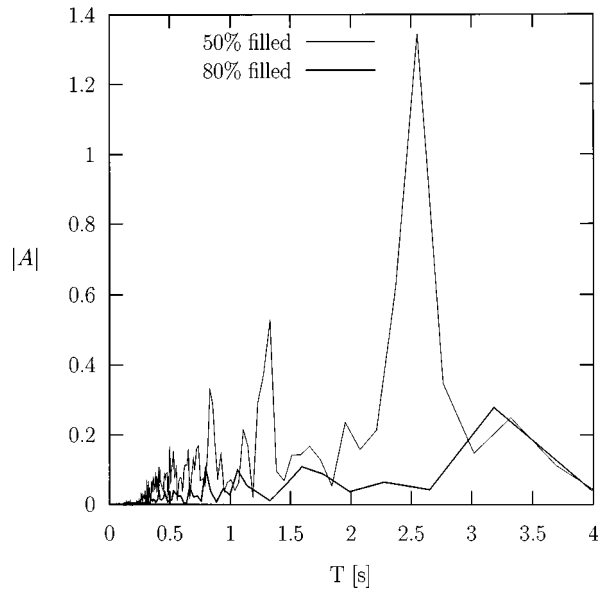

FIG. 4. Fourier transform of $q(t)$ of Fig. 3.

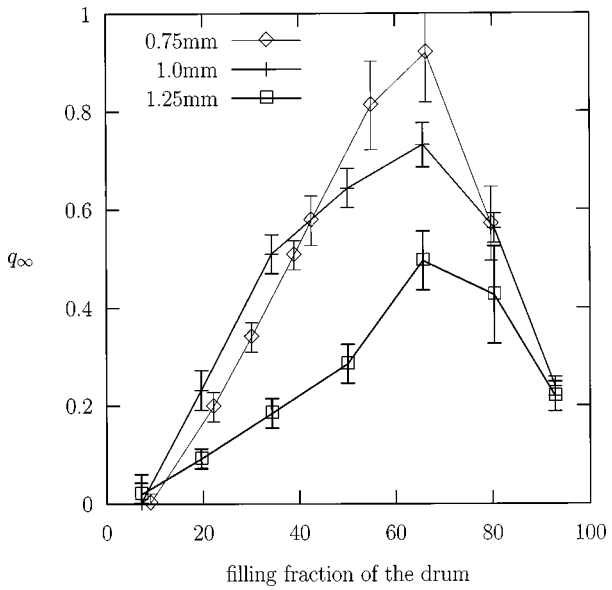

FIG. 5. The final amount of segregation for a concentration of 50% of small particles and three different size ratios.

make one revolution, i.e., to appear at the same spot again, given as

$$T=\frac{\alpha}{\Omega}+\frac{l}{\langle v\rangle}, \tag{8}$$

where α is the arc where the particle is in the solid block, l the length of the fluidized layer and $\langle v\rangle$ the average velocity of the particles in the fluidized layer. For a half-filled drum this gives $\alpha=\pi$ and $l=2R$. From this, we calculate $\langle v\rangle$ to be $\langle v\rangle=12.5$ cm/s in each case. This is in agreement with our detailed simulations where we get $\langle v\rangle=8.8\ldots17.7$ cm/s depending on the filling ratio and the particle sizes. The depth of the fluidized layer is determined as in Refs. 21 and 22 by looking at the velocity profile along a line through the center of the drum and perpendicular to the free surface. The depth of the fluidized layer is the distance from the free surface to the point where the velocity profile reaches its zero value.

In Fig. 3, the upper curve (thin line) corresponds to a half-filled cylinder. Due to the discrete particle number, the starting configuration might show a slight asymmetry in the spatial distribution of the particle sizes. This asymmetry will persist for some time due to the bad geometric mixing; therefore large fluctuations which slowly decrease in time are visible. For other filling ratios of the cylinder, the asymmetry in the beginning will decrease in time very fast due to the geometrical mixing. This is illustrated by the thick line in Fig. 3 which is for a volume filling fraction of 80% and, as expected, the fluctuations have a much smaller amplitude and do not show such a pronounced periodicity.

C. Dependence on the filling fraction

We will now turn to the pre-factor of the exponential fit in Eq. (7), q_∞, which quantifies the final amount of segregation and study its dependence on the volume filling fraction and on the particle size ratio. This is shown in Fig. 5 for three different particle sizes, corresponding to a size ratio of $\Phi=0.5,0.67$ and 0.83, respectively, and a concentration of small particles of 50%. For smaller particles, the final amount of segregation is higher for nearly all filling ratios of the cylinder which corresponds to a better segregated system.

Since the geometrical mixing will also cause mixing of the segregated core of small particles with the large particles, the best segregation should be achieved for zero mixing, see also Sec. III B. In our case where we have a fluidized layer with finite width, the best segregation occurs not for a half-filled cylinder, instead it occurs for a filling fraction of around 65%; see Fig. 5. This might be explainable in the following way: Our fluidized layer has a width of about three to four particles, which suggests that the best segregation occurs not for a half-filled cylinder; instead it occurs for a cylinder where the solid block under the fluidized layer occupies roughly 50% of the volume.

Concerning different concentrations of small particles, our parameter was normalized in such a way that the final amount of segregation should be independent of the volume fraction of small particles in the cylinder. We checked this numerically for a concentration of 50% and 33% and found a perfect agreement within the error bars. The speed of the segregation is characterized by t_c; see Eq. (7), stating that for $t=t_c$ the system has reached a segregation of 63% of the final value of q_∞. In Fig. 6, we plot the characteristic number of revolutions, defined as $n_c=\Omega t_c/2\pi$, as a function of the volume filling fraction of the cylinder for three different sizes of the small particles corresponding to particle size ratios of $\Phi=0.50,0.67$ and 0.83 again. The segregation times are significantly smaller for the smaller particles which is also found in experiments.[23] They also show a general trend of increasing with an increasing filling fraction. However, for a more than half-filled drum, where the exact value depends on the particle size due to the different width of the fluidized layers, the segregation becomes faster again. This can be explained as follows: Due to the nature of the geometrical mixing, an unmixed core will persist in the middle of the cylinder for a filling fraction greater than 50%. The

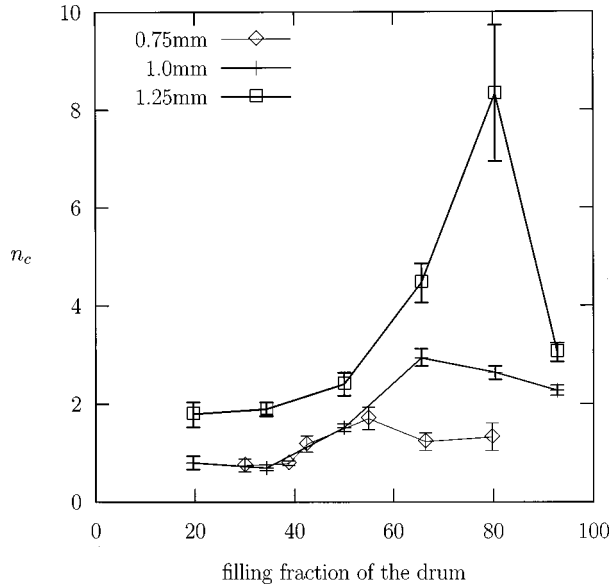

FIG. 6. Characteristic number of revolutions for segregation for a concentration of 50% of small particles.

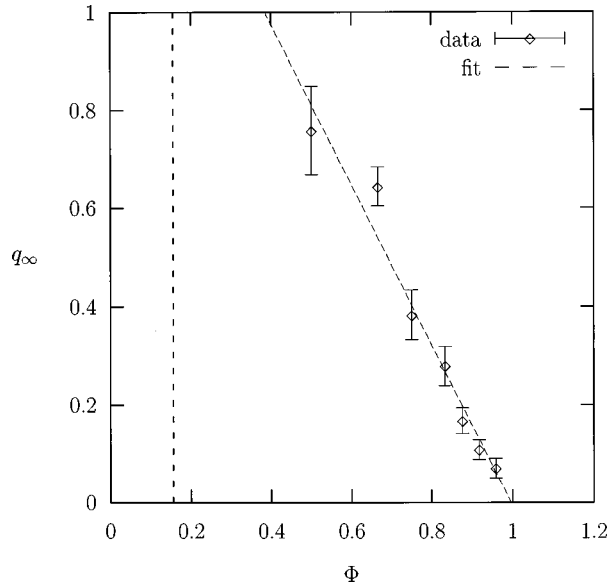

FIG. 7. The final amount of segregation as function of the particle size ratio $\Phi = r/R$ (the vertical dashed line denotes Φ_T).

exact number depends on the width of the fluidized layer which depends, e.g., on the rotation speed of the cylinder. Close to a filling fraction of one, only a small ring close to the cylinder wall can participate in the segregation process. Consequently, the final amount of segregation is small which agrees with Fig. 5, but this value is reached fast, therefore the segregation time, t_c, is small. The numerical data indicates that the filling fraction which corresponds to the maximal value of t_c decreases with decreasing particle size.

It is well known, that the segregation process is faster and more pronounced if the particle size ratio becomes smaller.[23] The results from a two-dimensional rotating drum model indicate that segregation is observed for an arbitrary small size ratio,[24] whereas the data from vertical shaking experiments suggest a cut-off ratio around $\Phi=0.5$.[25] In order to address this question, we show in Fig. 7 the final amount of segregation, q_∞, as a function of the particle size ratio, Φ, for a concentration of small particles and a volume filling fraction of 50%. Even though obtaining accurate data for values of Φ close to one is rather difficult due to the long segregation time, the data shown in Fig. 7 support the hypothesis from Ref. 24 that segregation will be present for any finite size difference. This was determined by using a linear fit of the form

$$q_\infty(\Phi) = c(\Phi - \Phi_0), \tag{9}$$

which gives $c = 1.6 \pm 0.1$ and $\Phi_0 = 1.00 \pm 0.02$ when all seven data points are used for the fit; shown as a dashed line in Fig. 7.

Due to our definition, the maximal achievable value for the final amount of segregation is $q_\infty = 1$. Therefore, for small size ratios, the behavior must deviate from the linear dependence which is already visible for the value for $\Phi=0.5$ which was obtained by interpolating between two filling fractions. Obtaining data points for even lower values of Φ is nearly infeasible by todays computers, due to the large demand on computer time caused by the large particle numbers. For values of $\Phi \leqslant \Phi_T := 2/\sqrt{3}$ (the wide dashed line in Fig. 7), we expect a completely different behavior since the small particles are then sufficiently small to propagate through the voids of a three-dimensional hexagonal packing. Please note that since we have a random packing, see Fig. 2, the threshold value should even be higher and Φ_T just serves as a lower bound.

D. Half-filled pre-set cylinder

In order to illustrate the interplay between mixing and segregation in more depth, we start with an initial configuration where the left half of the cylinder is purely composed out of large beads ($R = 1.5$ mm) and the right half out of small beads ($r = 1.0$ mm) giving a total number of 4420 particles (see Fig. 8, top left picture). After turning the drum counter-clockwise for 1.6 seconds at $\Omega = 15$ rpm, which would simply interchange the regions occupied by large and small particles if no mixing were present, the interface is still well defined and nearly a straight line (top right picture). After turning for 2.8 seconds, the interface between the large and small beads is still quite sharp, albeit it is not a straight line anymore. After the start of the rotation, it takes 0.23 s for the continuous flow to set in and from Sec. III B we recall that it takes roughly 2.65 s for a particle to undergo a full revolution. The tongue of small particles into the large ones at the center of the cylinder is the starting point of forming a core of small particles. After rotating for 5.3 s, which corresponds to the particle having undergone two full revolutions, the formation of a core of small (white) particles is even more pronounced. After having undergone three revolutions, $t = 7.8$ s, the shape of the interface between large and small particles close to the cylinder wall becomes even more diffusive. The segregation mechanism in the pre-set cylinder starts immediately, i.e., *no* mixing of the two components is necessary in order to obtain a radially segregated core of small particles. The final picture in Fig. 8 (bottom right) corresponds to 28 particle revolutions and shows a nearly symmetric, well segregated cluster of small particles. Also

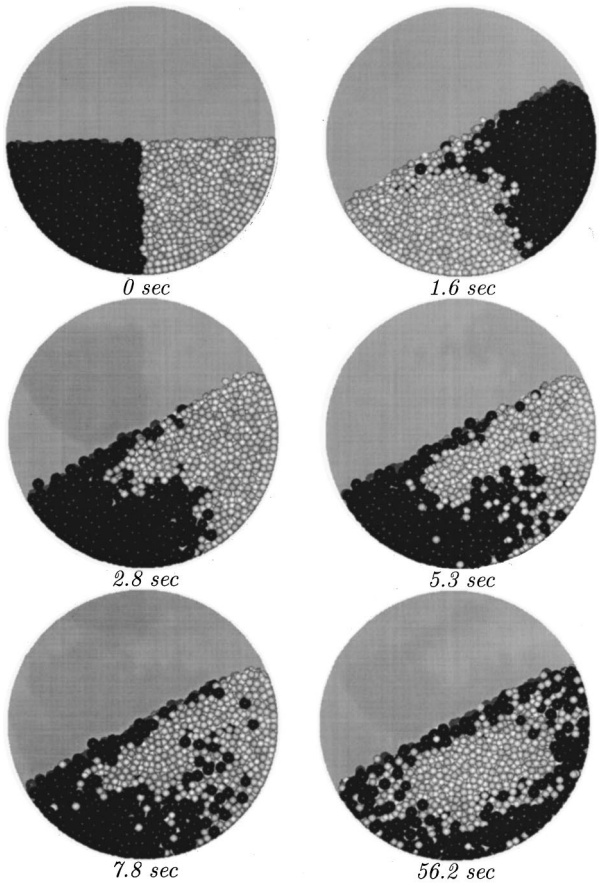

FIG. 8. Different snapshots of the cylinder with a starting condition, where initially all the small (large) particles are on the right (left) side of the cylinder (particle radii 1.0 mm and 1.5 mm).

note that hardly any large particles are found in the segregated core of small particles whereas smaller particles are still found close to the wall of the drum. We expect the latter effect to disappear when the drum is rotated for long enough times.

In order to determine the degree of mixing in the horizontal cylinder along the initially sharp vertical front we use a procedure proposed by Metcalfe *et al.*[4] We calculate the center of mass for each particle size, project it onto the free surface which is initially horizontal and calculate the distance of each of the two centers of mass. The time evolution of this distance, ξ_c, which was made dimensionless by dividing by the distance of the start configuration, is shown in Fig. 9. It corresponds to the configuration shown in Fig. 8, i.e., a half-filled cylinder containing an equal volume fraction of 1 mm and 1.5 mm particles. In Ref. 4, this procedure was used to show the mixing of mono-disperse particles in a rotating drum at a filling fraction of $f=39\%$. Since geometrical mixing is observed for this filling fraction, the centroid positions decayed in time and could be well approximated by

$$\xi_c(t)=\cos\left(\frac{2\pi t}{T}\right)e^{-t/\tau}, \tag{10}$$

where T stands for the period; see Eq. (8). On the contrary, no geometrical mixing is observed for mono-disperse particles in a half-filled drum which would correspond to a characteristic time $\tau=\infty$ in Eq. (10) and lead to nondecaying oscillations. For a binary particle mixture, the segregation process will lead to a decay of the distance of the two centroids in time for *any* filling fraction and we have chosen to present numerical results for counter-clockwise rotation and $f=50\%$ in Fig. 9 to illustrate this.

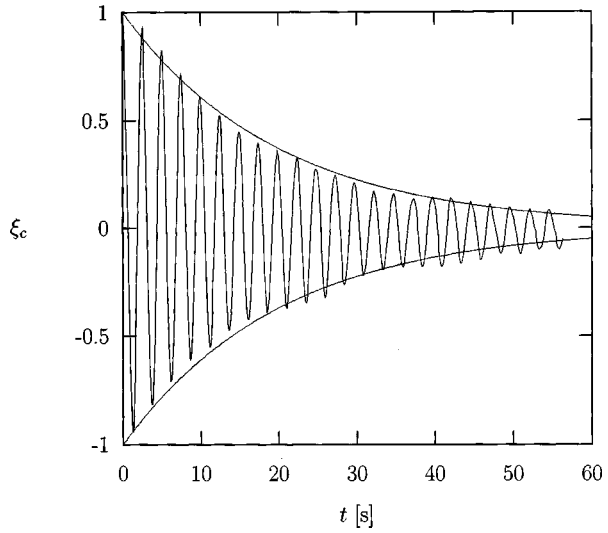

FIG. 9. Normalized centroid position projected onto the free surface of a half-filled cylinder with 1.0 mm and 1.5 mm particles.

The numerical data can be well fitted by an exponentially decaying oscillation according to Eq. (10). This gives $T=2.48$ s which is in excellent agreement with Fig. 4, and values of $\tau=20.7$ s for clockwise rotation and $\tau=20.1$ s for counter-clockwise rotation which are the same within the error bar. The exponentially decaying part was added to Fig. 9 as a dashed line. In the beginning, $t<20$ s, a slight asymmetry is visible towards negative values which was also observed in other numerical simulations using a two-dimensional geometrical model.[26] However, we could not determine by this procedure if the asymmetry persists in the long run and will lead to a final nonzero value for the centroid position since the deviations from the exponential fit were usually higher than the calculated offset of (0.004 ± 0.001) cm. Since the numerical data seems to indicate that a pure exponential decay is too slow in the beginning and too fast for longer times we also tried a stretched exponential decay of the form $e^{-(t/\tau)^{\beta}}$. This gives values of $\tau=(14.0 \pm 1.8)$ s and $\beta=0.88\pm0.05$, respectively. However, we can not rule out that the deviation of the exponential law may be due to the numerical noise and a more general statistical theory is needed to resolve this question.

The procedure described above to follow the centroid dynamics is not capable to determine the depth of the centroid position below the free surface due to the projection of the center of masses of each particle component onto the free surface. However, the last picture of Fig. 8 shows that the number of layers of large particles below and above the segregated cluster of small particles is not the same. This leads to different distances of the center of mass below the free surface for small and large particles. To determine its dy-

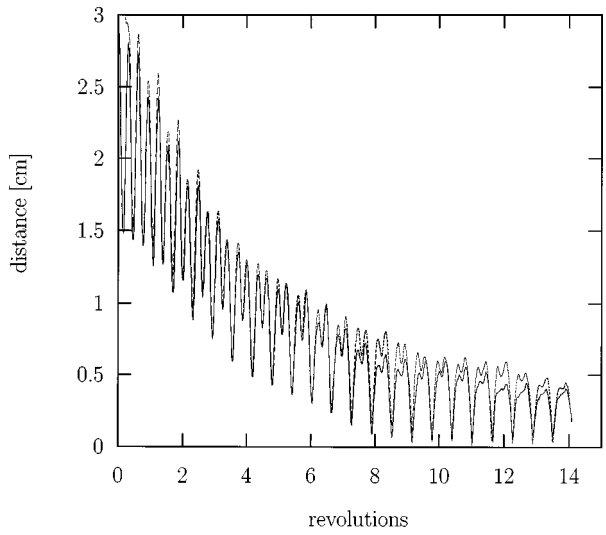

FIG. 10. The distance of the centers of a half-filled cylinder with 1.0 mm and 1.5 mm particles (- - - clockwise; —, counter-clockwise rotation).

namic, we plot in Fig. 10 the Euclidean distance of the two centroids. When properly shifted by $T/2$, the curves for clockwise and counter-clockwise rotations show a similar behavior where fluctuations are a little less pronounced for the latter case. The minima correspond to configurations similar to the one shown in the bottom right picture of Fig. 8 when the two centers of mass lie on a line which goes through the origin of the drum. Even though the minimal distance during the time evolution is close to zero, a nonzero value of 0.22 cm is estimated for the stationary state without oscillations.

IV. CONCLUSIONS

The main conclusions of this paper are as follows: When a rotating drum is operated in the continuous flow regime, our numerical results indicate that size segregation will take place for arbitrarily small differences in particle size. To quantify this result we introduced an appropriate order parameter, which allowed us to compare directly all different drum scenarios. From this we showed that the radial segregation process is faster and more pronounced for particles with a large size difference and that the final amount of segregation shows a linear dependence when approaching a particle size ratio of one; thus no threshold value for radial segregation exists, which was an unresolved question for a long time.

We also studied in detail the interplay between mixing and segregation in rotating cylinders for different volume filling fractions of the cylinder and found that the highest achievable segregation can be obtained for a slightly more than half-filled cylinder and therefore also least mixing. When compared to a system containing mono-disperse particles in the discrete avalanche regime, the observed differences could be attributed to the width of the fluidized layer leading to a partial destruction of the underlying, already segregated core, where the destruction increases with layer width.

When starting with an initial configuration that contains well-separated regions of small and large particles, for our setup no mixing of the components is necessary in order to obtain a radially segregated core. This inter-penetration process resembles a diffusion process and segregation starts immediately without undergoing a previous mixing of the two particle components. However, this might be different for other geometries.

ACKNOWLEDGMENTS

We would like to thank the HLRZ in Jülich and the HRZ Marburg for supporting us with a generous grant of computer-time on their Cray T3E and IBM SP2, respectively. Financial support by the Deutsche Forschungsgemeinschaft is gratefully acknowledged.

APPENDIX: ROLLING FRICTION

One of the most distinct properties of a glass bead is its ability to roll, therefore rolling had to be included into our model. The drawback was, that a glass bead would have had a Coulomb friction of zero with our frictional laws; i.e., a glass sphere would start to roll even on an infinitesimal inclined plane or a particle would roll on forever on every flat plane, which in reality clearly does not occur. For an ideal elastic particle, the deformation of the particle would be symmetric to the point of contact and therefore the resulting counter force of the plane would be exactly opposite to the gravitational force F_N for all times. In reality the deformation is not elastic, i.e., the deformation lags behind as is indicated in Fig. 11 for a particle on an ideal hard plane. The counter force of the plane F acting on the particle gets mediated by the deformation of the particle. The point where this force acts on is shifted slightly by r_0 to the back, the normal component of F compensates the gravitational force F_N exactly (otherwise the particle would bounce); leaving the tangential component of F which acts as rolling resistance which must be compensated by a dragging force for a particle with constant velocity on a flat plane. Also, simulation shows that the angle of repose is much too small in comparison with experiment without rolling resistance. To overcome this weakness we add rolling resistance[27] to our model, see Fig. 11, by using

$$F_r = \frac{r_0}{R} F_N . \tag{A1}$$

Here the rolling resistance r_0 is a constant material parameter and results from the slight viscoelasticity of the materials. r_0 is of the order of $10^{-3}-10^{-5}$ mm for most of the materials. For particle–particle interactions, we take the same law for rolling resistance as for particle–wall interactions.

The rolling resistance acts as a net torque constructed out of a force couple F_r with

$$F_r = |F_N| \frac{r_0}{R} (\hat{n} \times \hat{s}). \tag{A2}$$

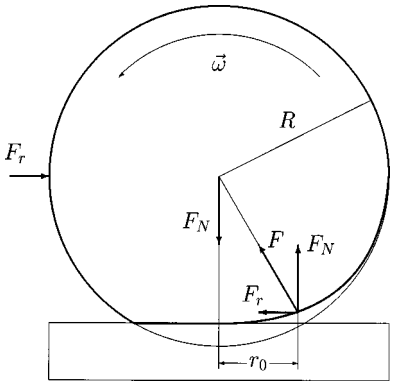

FIG. 11. Viscoelastic rolling sphere on a hard surface.

We also have to consider that the rolling resistance can only decrease angular momentum, but never revert it. And so we have to limit F_r by the quantity that would reduce the angular momentum to zero within the next time step, namely,

$$F_{r_{\max}} = \frac{2}{5} mR \cdot ((\hat{n} \times \hat{s}) \cdot \boldsymbol{\omega}) / (\Delta t). \tag{A3}$$

For the torque we therefore get

$$T_r = R \cdot \min(F_r, F_{r_{\max}}). \tag{A4}$$

As can already be seen from the definition of the rolling resistance, Eq. (A1), the rolling friction on small particles will be higher than on large particles which was also observed by studying one particle on a bumpy line[28] and in experiments with glass marbles. To illustrate this fact, we show in Fig. 12 the dependency of the angle of repose on the rolling friction parameter r_0. The higher friction of smaller particles results in a steeper slope of the angle of repose in Fig. 12. An important result of this is that we can adjust the rolling friction in such a way that small and large glass beads have the same angle of repose as is seen in experiments for glass beads.[17,18] Also, one clearly sees that for small r_0 the slope of the angle of repose $\delta\Theta/\delta r_0$ is proportional to r_0, which results from the law of rolling resistance Eq. (A1).

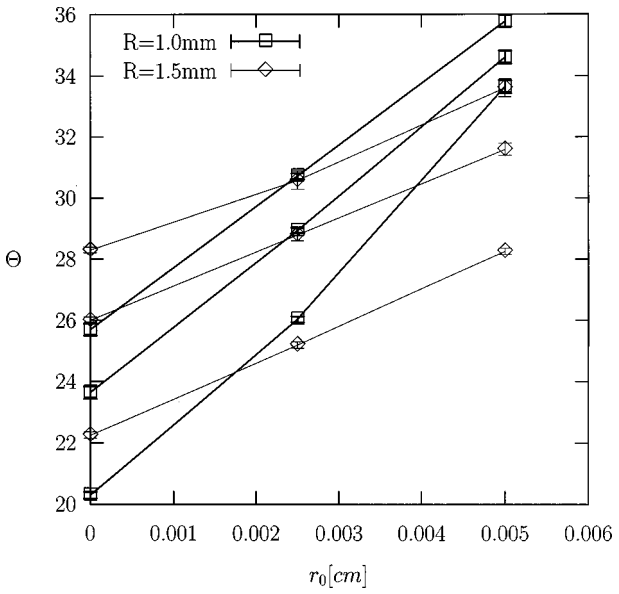

FIG. 12. Angle of repose for different friction coefficients and particle diameter of 1.0 mm and 1.5 mm for three different values of μ ($\mu = 0.1$, 0.2, and 0.3 from bottom to top).

[1] N. Nityanand, B. Manley, and H. Henein, ''An analysis of radial segregation for different sized spherical solids in rotary cylinders,'' Metall. Trans. B **17**, 247 (1986).
[2] J. Rajchenbach, ''Flow in powders: From discrete avalanches to continuous regime,'' Phys. Rev. Lett. **65**, 2221 (1990).
[3] M. Caponeri, S. Douady, S. Fauve, and C. Laroche, ''Dynamics of avalanches in a rotating cylinder,'' in *Mobile Particulate Systems*, edited by E. Guazzelli and L. Oger (Kluwer, Dordrecht, 1995), p. 331.
[4] G. Metcalfe, T. Shinbrot, J. J. McCarthy, and J. M. Ottino, ''Avalanche mixing of granular solids,'' Nature (London) **374**, 39 (1995).
[5] B. A. Peratt and J. A. Yorke, ''Continuous avalanche mixing of granular solids in a rotating drum,'' Europhys. Lett. **35**, 31 (1996).
[6] S. N, Dorogovtsev, ''Avalanche mixing of granular solids,'' Europhys. Lett. **41**, 25 (1998).
[7] E. Clément, J. Rajchenbach, and J. Duran, ''Mixing of a granular material in a bidimensional rotating drum,'' Europhys. Lett. **30**, 7 (1995).
[8] F. Cantelaube and D. Bideau, ''Radial segregation in a 2D Drum: an experimental analysis,'' Europhys. Lett. **30**, 133 (1995).
[9] G. Baumann, I. M. Janosi, and E. D. Wolf, ''Surface properties and flow of granular material in a two-dimensional rotating drum model,'' Phys. Rev. E **51**, 1879 (1995).
[10] K. M. Hill, A. Caprihan, and J. Kakalios, ''Bulk segregation in rotated granular material measured by magnetic resonance imaging,'' Phys. Rev. Lett. **78**, 50 (1997).
[11] C. M. Dury and G. H. Ristow, ''Radial segregation in a two-dimensional rotating drum,'' J. Phys. I **7**, 737 (1997).
[12] G. H. Ristow, ''Particle mass segregation in a two-dimensional rotating drum,'' Europhys. Lett. **28**, 97 (1994).
[13] G. Metcalfe and M. Shattuck, ''Pattern formation during mixing and segregation of flowing granular materials,'' Physica A **233**, 709 (1996).
[14] D. V. Khakhar, J. J. McCarthy, and J. M. Ottino, ''Radial segregation of granular mixtures in rotating cylinder,'' Phys. Fluids **9**, 3600 (1997).
[15] H. E. Rose, ''A suggested equation relating to the mixing of powders and its application to the study of the performance of certain types of machine,'' Trans. Inst. Chem. Eng. **37**, 47 (1959).
[16] R. P. Behringer, ''Mixed predictions,'' Nature (London) **374**, 15 (1995).
[17] O. Zik, D. Levine, S. G. Lipson, S. Shtrikman, and J. Stavans, ''Rotationally induced segregation of granular materials,'' Phys. Rev. Lett. **73**, 644 (1994).
[18] C. M. Dury, G. H. Ristow, J. L. Moss, and M. Nakagawa, ''Boundary effects on the angle of repose in rotating cylinders,'' Phys. Rev. E **57**, 4491 (1998).
[19] S. F. Foerster, M. Y. Louge, H. Chang, and K. Allia, ''Measurements of the collision properties of small spheres,'' Phys. Fluids **6**, 1108 (1994).
[20] D. V. Khakhar, J. J. McCarthy, T. Shinbrot, and J. M. Ottino, ''Transverse flow and mixing of granular materials in a rotating cylinder,'' Phys. Fluids **9**, 31 (1997).
[21] M. Nakagawa, S. Altobelli, A. Caprihan, E. Fukushima, and E.-K. Jeong, ''Non-invasive measurements of granular flows by magnetic resonance imaging,'' Exp. Fluids **16**, 54 (1993).
[22] G. H. Ristow, ''Dynamics of granular materials in a rotating drum,'' Europhys. Lett. **34**, 263 (1996).
[23] J. C. Williams, ''The segregation of particulate materials. A review,'' Powder Technol. **15**, 245 (1976).
[24] G. Baumann, I. Janosi, and D. E. Wolf, ''Particle trajectories and segregation in a two-dimensional rotating drum,'' Europhys. Lett. **27**, 203 (1994).
[25] L. Vanel, A. D. Rosato, and R. Dave, ''Rise-times regimes of a large sphere in vibrated bulk solids,'' Phys. Rev. Lett. **78**, 1255 (1997).
[26] G. Baumann, Ph.D. thesis, University of Duisburg, Duisburg, Germany, 1997.
[27] K. L. Johnson, *Contact Mechanics* (Cambridge University Press, Cambridge, 1985).
[28] G. H. Ristow, F.-X. Riguidel, and D. Bideau, ''Different characteristics of the motion of a single particle on a bumpy inclined line,'' J. Phys. I **4**, 1161 (1994).